# A DFT study of gas adsorption (NO, $NO_2$)on metal oxides (CuO, $Ag_2O$) modified $Ti_3C_2O_2$ monolayer

JiaHui Su[1,2], Xin Liu[1,2]*, Hanmei Zhang[1,2], Bing Zhao[1,2], Yue Feng[3], Chao Wang[4], Tao Shen[2]*

**Abstract**

The adsorption properties of five gases on metal oxides (CuO, $Ag_2O$) modified $Ti_3C_2O_2$ were studied by the first-principles density functional theory. The gas sensitivity of nitric oxide, ammonia, nitrogen dioxide, methane, and formaldehyde on metal oxides (CuO, $Ag_2O$) modified $Ti_3C_2O_2$ was systematically discussed on the aspects of adsorption energy, the density of state, and electronic localization function and desorption time. The results prove that metal oxides (CuO, $Ag_2O$) modified could enhance the adsorption abilities of $Ti_3C_2O_2$. The adsorption capacity of CuO-modified $Ti_3C_2O_2$ is $NH_3$>NO>$NO_2$>$CH_2O$>$CH_4$, and the adsorption capacity of $Ag_2O$-modified $Ti_3C_2O_2$ is NO>$NO_2$>$CH_2O$>$NH_3$>$CH_4$. The $NO_2$ adsorption capacity $Ag_2O$-modified $Ti_3C_2O_2$ is 11.24 times than pure $Ti_3C_2O_2$. By comparison, CuO-modified $Ti_3C_2O_2$ is more suitable for capturing NO gas than $Ag_2O$-modified $Ti_3C_2O_2$, and the former exhibits chemically adsorbed. Considering the results, CuO and $Ag_2O$ modified $Ti_3C_2O_2$ can be used as oxynitride gas sensors.

**Key Words:** NO gas sensor; $NO_2$ gas sensor; DFT; metal oxides modified; $Ti_3C_2O_2$ MXene.

---

[1] *College of science, Harbin University of Science and Technology, Harbin 150080, P. R. China.*

[2] *Heilongjiang Province Key Laboratory of Laser Spectroscopy Technology and Application, Harbin University of Science and Technology, Harbin 150080, China;*

[3] *Key Laboratory of Engineering Dielectrics and Its Application, Ministry of Education, Harbin University of Science and Technology, Harbin, 150080, China；*

[4] *School of Engineering, University of Kent, Canterbury CT2 7NT, UK*

*Corresponding author E-mails: liux870118@hrbust.edu.cn; taoshenchina@163.com*

## 1. Introduction

Gas detection plays a vital role in monitoring and exploration of toxic gases. The detection of toxic gas molecules is of great significance in causing environmental pollution and public problems [1]. There are two sources of oxynitride, natural and industrial manufacture. In nature, it is mainly produced by decomposing organic matter in soil and oceans. Most of the way of industrial manufacture come from the combustion process of fossil fuels. Oxynitride, mainly NO and $NO_2$, are an important cause of photochemical smog and acid rain. NO is highly toxic, and the presence of a large amount of NO gas in the air will cause health problems to the human body and may also cause environmental pollution [2-4]. In addition to affecting daily life, $NO_2$ can also damage the atmospheric environment [5].

In recent years, with the rapid development of materials science, gas-sensing technology based on nanoscale gas-sensitive materials has made significant breakthroughs. New two-dimensional nanomaterials such as graphene, boron nitride, and MXenes have attracted attention because of their unique geometric structures and high specific surface areas. So far, many remarkable achievements have been made in the field of gas sensitization [6-9]. Among them, $Ti_3C_2O_2$ is particularly outstanding in the development of gas sensors due to its rich adsorption sites and stable structure. By managing strain, it is expected to become a feasible test material for gas sensors. Kong et al. found that $Ti_3C_2O_2$ and $Ti_3C_2F_2$ with point vacancies have high sensitivity to $SO_2$ [10]. Zeng et al. mentioned in their research that $Ti_3C_2T_X$ has good sensing ability for NO and $NO_2$ [11]. Unfortunately, nitride gas does not react well enough to gas sensors made of pure $Ti_3C_2O_2$. Weng et al. found that monolayer $Ti_3C_2O_2$ on $NO_2$ is physical adsorption [12]. Therefore, it is urgent to modify $Ti_3C_2O_2$ MXenes to improve its adsorption performance.

Fortunately, studies have shown that improving gas sensitivity on two-dimensional materials can be achieved by modifying surface transition metal oxides. Specifically, it is by introducing more adsorption sites or building heterostructures at the contact interfaces of different materials [13-15]. For example, CuO-modified graphene is considered as an excellent sensor for $H_2S$ detection [16]. The adsorption of $C_2H_2$, $NH_3$

and NO gases by metal (CuO, $Ag_2O$) modified $MoTe_2$ has been studied [17]. Among them, the adsorption performance of $MoTe_2$ modified by $Ag_2O$ and CuO is significantly improved, which provides a theoretical basis for metal modification. The sensors based on graphene decorated with CuO nanorods showed best sensitivity and selectivity to $H_2S$ gas [18]. Ghasemi A R et al. used thin film of $Ag_2O$-nanoparticles MWCNTs for specific detection of methane, the fabricated sensor has significant novelties such as specificity, reproducibility, high sensitivity, more improved detection limit and short response time [19]. These reports show that CuO and $Ag_2O$ have the potential to improve the gas-sensing properties of two-dimensional materials. However, to the best of our knowledge, a study of theoretical calculation research on the gas sensing properties of metal oxide (CuO, $Ag_2O$) modified $Ti_3C_2O_2$ for five gases has not been reported to date.

Combined with previous studies on $Ti_3C_2O_2$ gas sensitivity, this study analyzed the interaction between metal (CuO, $Ag_2O$) modified $Ti_3C_2O_2$ MXene and five gases (NO, $NH_3$, $NO_2$, $CH_4$, and $CH_2O$) gas molecular systems through DFT research. First, the most stable position of metal (CuO, $Ag_2O$) modified $Ti_3C_2O_2$ is analyzed. Subsequently, the reaction mechanism of the interaction between metal (CuO, $Ag_2O$) modified $Ti_3C_2O_2$ and five gases were studied. The results show that the $Ti_3C_2O_2$ structure modified by the most stable metal (CuO, $Ag_2O$) could improve the adsorption performance of oxynitride gas. Our research provides academic impetus for the advancement of oxynitride sensors.

## 2. Computational details

DFT calculations are performed in the Vienna Ab initio Simulation Package (VASP) [20] to add pseudopotentials using Projector Augmented Waves (PAW) to characterize the interactions between electrons and ions [21]. The Perdew-Burke-Ernzerhof (PBE) function of the generalized gradient approximation (GGA) is used for geometry optimization for all calculations [22,23]. Calculations converged using a plane wave cutoff energy of 520 eV and a force of -0.05 eV/Å. The self-consistent field convergence accuracy was set to $1.0\times10^{-6}$ Ha. During the structural optimization process, 4×4×1 Monkhorst-Pack K-points were used to sample Brillouin. In this study,

we use a 3×3×1 $Ti_3C_2O_2$ monolayer. To obtain a single layer of $Ti_3C_2O_2$ and eliminate the interaction between adjacent layers, we set the thickness of the vacuum layer to 20Å [24]. Considering the interaction between the substrate surface and gas molecules, VASKIT was used to immobilize the two substrates [25]. When analyzing the interaction between gas molecules and matrix, all charges before and after adsorption of gas molecules on the matrix were distinguished, and CT between gas molecules and matrix was evaluated by Bader charge calculation [26-30].

The energy released during the surface bonding of metal and $Ti_3C_2O_2$ is denoted as $E_{bind}$, which is defined by equation 1:

$$E_{bind}=E_{metal\text{-}MXenes}-E_{metal}-E_{MXenes} \quad (1)$$

where $E_{metal}$, and $E_{MXenes}$ refer to the total energy of the metal, and pure $Ti_3C_2O_2$ monolayer, respectively. The $E_{metal\text{-}MXenes}$ refer to the total energy of the metal modified $Ti_3C_2O_2$ system.

And then equation 2 calculates the adsorption energy $E_{ads}$:

$$E_{ads}=E_{metal\text{-}MXenes\text{-}gas}-E_{gas}-E_{metal\text{-}MXenes} \quad (2)$$

where the $E_{metal\text{-}MXenes\text{-}gas}$ and $E_{gas}$ refer to the energy after the system adsorbs the gas and the energy of the gas. If $E_{ads}$ is less than 0, the process is spontaneous. And energy is released during the reaction.

To analyze the charge transfer of individual atoms during the gas adsorption process, $Q_t$ is calculated from equation 3:

$$Q_t=Q_{after}-Q_{before} \quad (3)$$

where $Q_{after}$ in equation 3 is the net charge of the atom after adsorption, and $Q_{before}$ is the net charge of the atom before adsorption. When $Q_t$ is less than 0, it means that the atom has lost electrons. In the opposite case, the atom receives electrons.

## 3. Results and discussion

### *3.1 $CuO/Ag_2O$ modified $Ti_3C_2O_2$ monolayer*

The most stable single-layer $Ti_3C_2O_2$ structure is shown in Figure 1. The lattice parameter of the $Ti_3C_2O_2$ cell is 3.01Å, which is relatively consistent with previous studies [31].

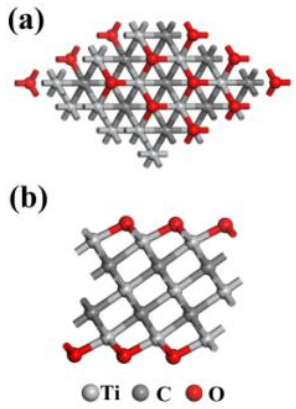


Figure 1. Top and side views of unadulterated $Ti_3C_2O_2$.

We considered a total of four different modification sites to obtain the most stable structure of CuO-modified $Ti_3C_2O_2$ and three different modification sites to obtain the most stable structure of $Ag_2O$-modified $Ti_3C_2O_2$. CuO-modified $Ti_3C_2O_2$ as shown in Figure 2(a-h), including between the Ti atom and the C atom (Figure 2a-b), between the Ti atom and the O atom (Figure 2g-h), top site above the Ti atom (Figure 2c-d), and top site above the O atom (Figure 2e-f). Considering that Cu and O atoms will have different effects when connected to different atoms, eight models are established. Comparing with Figure 2b, it can be found that the Cu atom in Figure 2a is originally connected with the C atom, which is close to the Ti atom, and the optimized Cu atom is bonded with the O atom, which is relatively far away. The Cu atom in Figure 2c is slightly shifted by the action of two O atoms near the Ti atom, while no such phenomenon is seen in Figure 2d. In Figure 2e, the O of the O functional group of $Ti_3C_2O_2$ is originally connected with the O atom of CuO, and the structure was optimized to become the O connection of Cu atom and the functional group. Therefore, Figure 2e looks like Figure 2f. A similar situation also appears in Figure 2h.

The most stable structure of $Ag_2O$-modified $Ti_3C_2O_2$, as shown in Figure 2(i-k), including between the O atom and the Ag atom (Figure 2i), between the Ti atom and the Ag atom, the Ag atom and the C atom (Figure 2j), between the Ti atom and the Ag atom, the Ag atom and the O atom (Figure 2k). Comparing with Figure 2j and Figure 2k, it can be found that the Ag atom is connected with the O atom. Therefore, Figure 2k looks like Figure 2i. A similar situation also appears in Figure 2j.

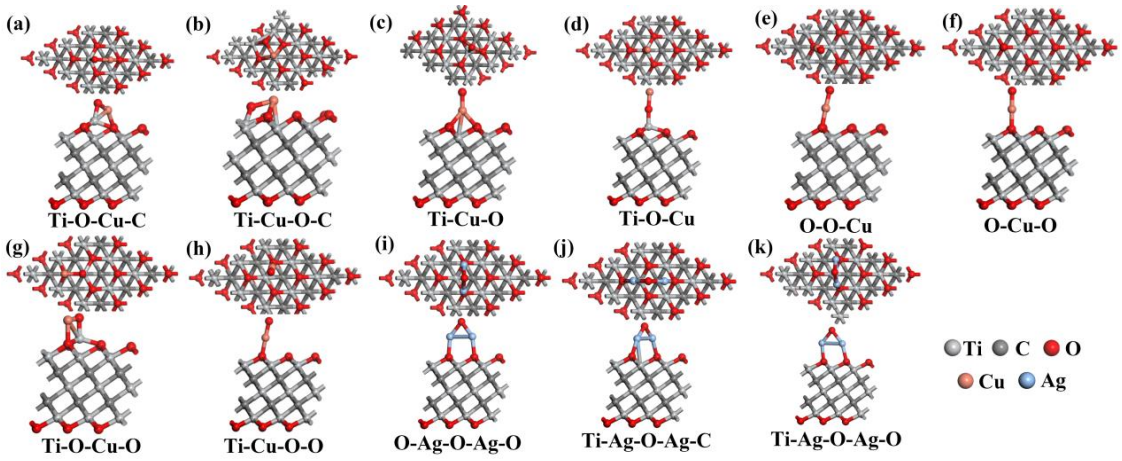


Figure 2. Top view and side view of $Ti_3C_2O_2$ modified by CuO and $Ag_2O$ at different sites.

To describe the energy released during the surface bonding process between CuO, $Ag_2O$ and $Ti_3C_2O_2$, and to express the stability of the structure, Figure 3 represents the amount of energy released. Among the eight CuO-modified $Ti_3C_2O_2$ models in Figure 3a, the Ti-O-Cu-C model has the smallest $E_b$ value (- 2.13 eV), that is the most energy released in the process. The Ti-O-Cu-O model is similar to the Ti-O-Cu-C model. The difference is that the Cu atom of the former is bound to the O atom which is closer to the Ti atom, while the latter is the distant O atom. Therefore, the most stable structure is shown in Figure 2a from the perspective of the energy released during the surface bonding process of CuO and $Ti_3C_2O_2$.

Among the three $Ag_2O$-modified $Ti_3C_2O_2$ models, the O-Ag-O-Ag-O model has the smallest $E_b$ value (-2.32 eV) in Figure 3b, that is, the most energy is released during the process. The Ti-Ag-O-Ag-O model is similar to the O-Ag-O-Ag-O model. The difference is that the structure of the former has slight deformations. From the perspective of the energy released during the surface bonding of $Ag_2O$ and $Ti_3C_2O_2$, the most stable structure is shown in Figure 2i.

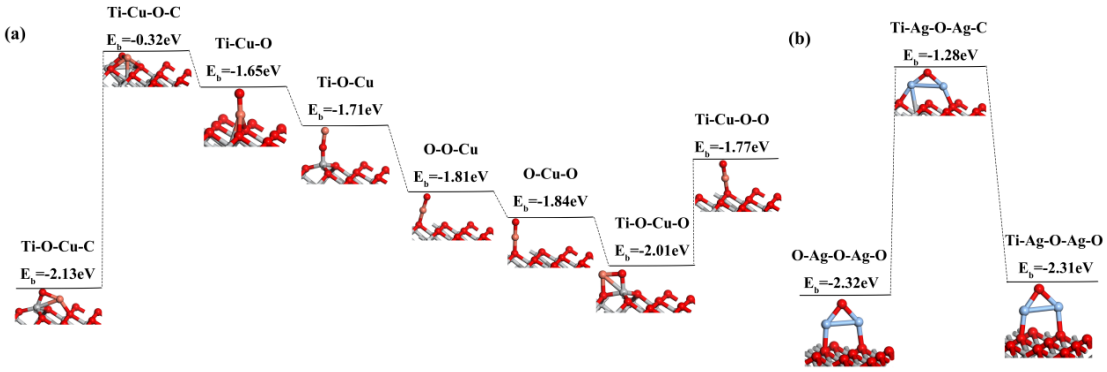


Figure 3. The released energy when CuO or $Ag_2O$ binds to $Ti_3C_2O_2$ at different sites

For the purpose of understanding the behavior of CuO and $Ag_2O$ modified $Ti_3C_2O_2$, calculation of the density of state (DOS), partial density of states (PDOS), the electron localization function(ELF), and average charge transfer. Figure 4a shows DOS before and after CuO modification. We found new peaks near -1.26 eV and -0.75 eV. According to the PDOS of Figure 4b, the O-2p orbital in $Ti_3C_2O_2$ hybridized with the Cu-3d orbital near -1.26 eV and -0.75 eV, possibly bonding between the O and Cu atoms. To further analyze the influence of CuO on the original $Ti_3C_2O_2$, ELF is calculated, as shown in Figure 4c. Corresponding to Figure 4b, the bonding interaction between the Cu atom and the O atom in $Ti_3C_2O_2$. According to the average charge transfer of different atoms of Ti-O-Cu-C in Figure 4d, it can be found that there are both electron inflow and outflow in CuO, which is related to the short distance between CuO and $Ti_3C_2O_2$. Meanwhile, for the $Ag_2O$ modification model, new peaks were found near -2.40 eV and -0.20 eV in DOS before and after $Ag_2O$ modification which can be seen in Figure 4e. According to the PDOS in Figure 4f, the O-2p orbital in $Ti_3C_2O_2$ hybridizes with the Ag-4d orbital around -2.40 eV and -0.20 eV. Figure 4g is consistent with the results analyzed in Figure 4f. There is a bonding interaction between the O atoms in $Ti_3C_2O_2$ and the Ag atoms in $Ag_2O$. According to the average charge transfer of different atoms of O-Ag-O-Ag-O in Figure 4h, it can be found that there are both electrons flowing in and electrons flowing out of $Ag_2O$.

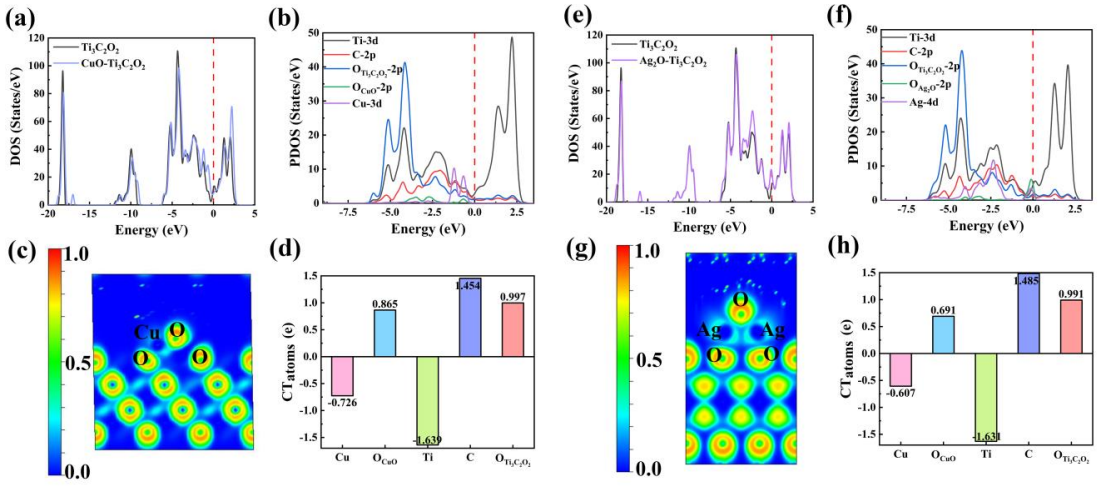


Figure 4. (a-d)TDOS, PDOS, ELF, and average charge transfer of Ti-O-Cu-C.

(e-h)TDOS, PDOS, ELF, and average charge transfer of O-Ag-O-Ag-O.

### *3.2 Adsorption of $CuO/Ag_2O$ modified $Ti_3C_2O_2$ monolayer to gas molecules*

To understand the adsorption behavior of five gas molecules on $CuO/Ag_2O$ modified $Ti_3C_2O_2$ monolayers, the geometric optimization and electronic properties of these adsorption systems were studied deeply. Adsorption energy, charge exchanged, DOS, and ELF were calculated.

Figure 5 shows the adsorption of five gases on the superior adsorption sites of CuO-modified and $Ag_2O$-modified $Ti_3C_2O_2$ monolayer, respectively. When $NH_3$ gas and $CH_2O$ gas are adsorbed on Ti-O-Cu-C, the Cu-O bond in CuO is broken. When NO gas and $CH_2O$ are adsorbed on O-Ag-O-Ag-O, the Ag-O bond in $Ag_2O$ is broken. It is obvious that there is still a distance between the $CH_4$ gas and both substrates.

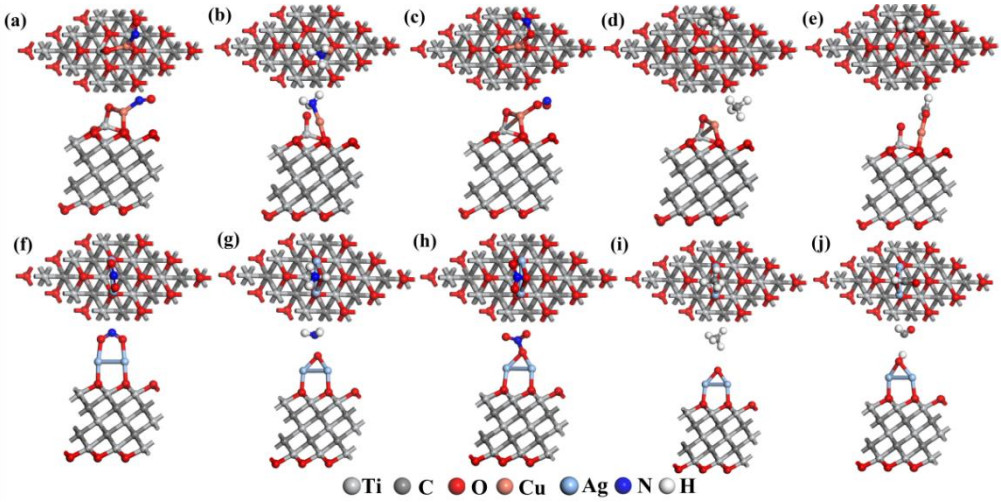


Figure 5. (a-e)five gases adsorption on Ti-O-Cu-C. (f-j)five gases adsorption on

O-Ag-O-Ag-O.

The adsorption energy and adsorption distance of five gases at Ti-O-Cu-C and O-Ag-O-Ag-O were presented in the Figure 6. The adsorption energy less than 0 means that the adsorption of gas by the substrate does not require energy from the outside world, but releases energy to the outside world. This means that the process is conducive to energy and is considered an exothermic process. The adsorption energies of pure $Ti_3C_2O_2$ for five gases calculated by our research group are -0.31 eV, -0.283 eV, 0.202 eV, -0.183 eV and -0.075 eV which are consistent with the results obtained by us and other researchers [9,11]. It can be seen from Figure 6a shows that the gas adsorption energies of NO, $NH_3$, $NO_2$, $CH_4$, and $CH_2O$ are −1.44 eV, −1.59 eV, −1.03 eV, -0.26 eV, and −0.83 eV, separately. Although the adsorption energy of $NH_3$ on Ti-O-Cu-C is the largest, $NH_3$ also causes the bond between the Cu atom and the O atom of CuO to break. The adsorption distance of $CH_4$ gas is the longest among the five gases, and its adsorption energy is also the smallest among all gases. The smaller adsorption energy may be caused by the longer adsorption distance. Compared with before modification, the adsorption effect is improved, and the $E_{ads}$ of $CH_4$ are enhanced by 42%, but it still appears as physical adsorption [2]. On the contrary, $E_{ads}$ for NO and $NO_2$ are about 4.64 times and 5.59 times higher than $Ti_3C_2O_2$. $E_{ads}$ of NO is -1.44 eV, while that of $NO_2$ is -1.03 eV. Meanwhile, the bond length between the N atom in NO and the Cu atom in CuO is 1.790 Å, while the bond length between the O atom in $NO_2$ and the Cu atom in CuO is 1.937 Å. In general, the adsorption effect of NO is better than that of $NO_2$.

In Figure 6b, the adsorption distance of $CH_4$ gas in the O-Ag-O-Ag-O structure is also the longest among the five gases, which is the same as Ti-O-Cu-C. The $E_{ads}$ of $NO_2$ is about 11.24 times higher than that of pure $Ti_3C_2O_2$. At the same time, the distance between N atoms in $NO_2$ and O atoms in $Ag_2O$ is 1.399Å. $Ag_2O$-modified $Ti_3C_2O_2$ has a better adsorption effect on $NO_2$ gas. The adsorption energy of NO is the largest of the five gases, but the structure of $Ag_2O$ changed. While maintaining the substrate, CuO-modified $Ti_3C_2O_2$ is more suitable for capturing NO gas than $Ag_2O$-modified $Ti_3C_2O_2$, and it is chemically adsorbed.

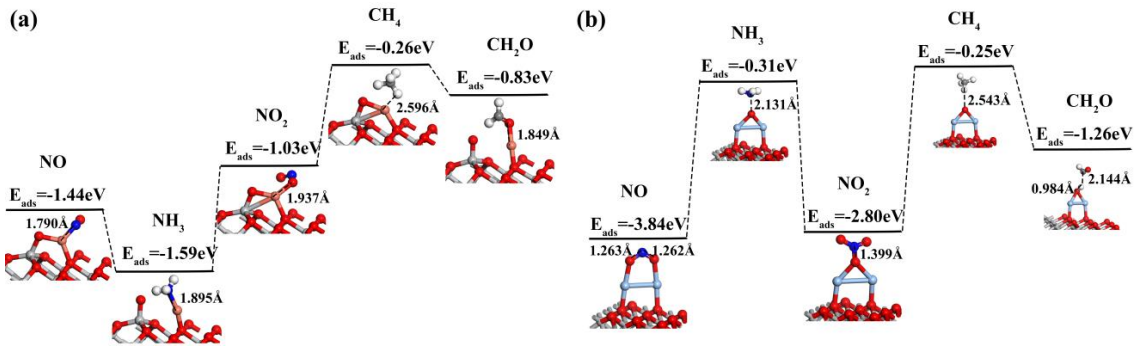


Figure 6. Adsorption energy and adsorption distance of five gases at (a) Ti-O-Cu-C and (b) O-Ag-O-Ag-O.

Because of the chemical adsorption characteristics of gas molecules on the matrix surface, the electronic properties of the matrix alteration during the examination of gas sensors. DOS analysis is a competent method for profoundly understanding electronic behavior [32,33]. Figure 7 depicts the density of states (DOS) of the five gases adsorped on CuO/$Ag_2O$ modified $Ti_3C_2O_2$ systems, as well as the orbital DOS, to illustrate the modified electronic property of the CuO/$Ag_2O$ modified $Ti_3C_2O_2$ by five gases adsorption. For convenience, the position of the dashed line (0 eV) is used as the Fermi level in the DOS diagram. In Figure 7, the interatomic interactions can be to a higher degree analyzed through the distribution of PDOS. The overlapping peaks between varying orbitals over a large range can be attributed to the strong inter-orbital hybridization.

Figure 7a shows that the TDOS after NO adsorption rises in the Fermi level state, which means the conductivity increases. For Ti-O-Cu-C, it can be observed that the TDOS increases significantly in a small range from -9.16 eV to -8.04 eV after NO adsorption. The hybridization of N-2p and Cu-3d orbitals near -13.08 eV, -8.93 eV, -1.87 eV, and 0.13 eV, indicating interaction between them. In Figure 7b, the N-2p orbital is hybridized with the Cu-3d orbital near -6.21 eV. For $NO_2$ adsorbed on Ti-O-Cu-C, it can be seen from Figure 7c that the overlapping orbits near -2.90 eV and -0.75 eV are mainly composed of O-2p orbits in $NO_2$ and Cu-3d orbits in CuO, indicating the interaction between them. Regarding $CH_4$, it should be specifically noted that the nearly unchanged TDOS depicted in Figure 7d figures that the sensitive detection of $CH_4$ on Ti-O-Cu-C is unfavorable. Likewise, the adsorption of $CH_4$ on

Ti-O-Cu-C is relatively poor, and its PDOS shows not much substantial interaction in Figure 7d. In Figure 7e, the PDOS of $CH_2O$, only O-2p and Cu-3d orbitals appear peaks at the same energy level (-3.24 eV and 1.46 eV).

For O-Ag-O-Ag-O in Figure 7f, the overlapping orbitals near -8.53 eV, -3.60 eV, -3.18 eV, -2.32 eV and -1.24 eV are mainly composed of O-2p orbitals in NO and Ag-4d orbitals in $Ag_2O$, indicating interaction between them. Figure 7h shows that TDOS has new peaks at -8.26 eV, -7.38 eV and -10.58 eV after $NO_2$ adsorption. It can be seen from PDOS that it is contributed by O-2p in $Ag_2O$ and N-2p orbitals in $NO_2$ gas, indicating interaction between them. The possible bonding of the N atom of NO and Cu atom is illustrated in Figure 7a. These state hybridizations verify the strong orbital interaction in the newly formed Cu-N bonds, confirming their strong binding force. The analysis of the relationship between NO and $NO_2$ and the substrate is consistent with the conclusion in the previous paper.

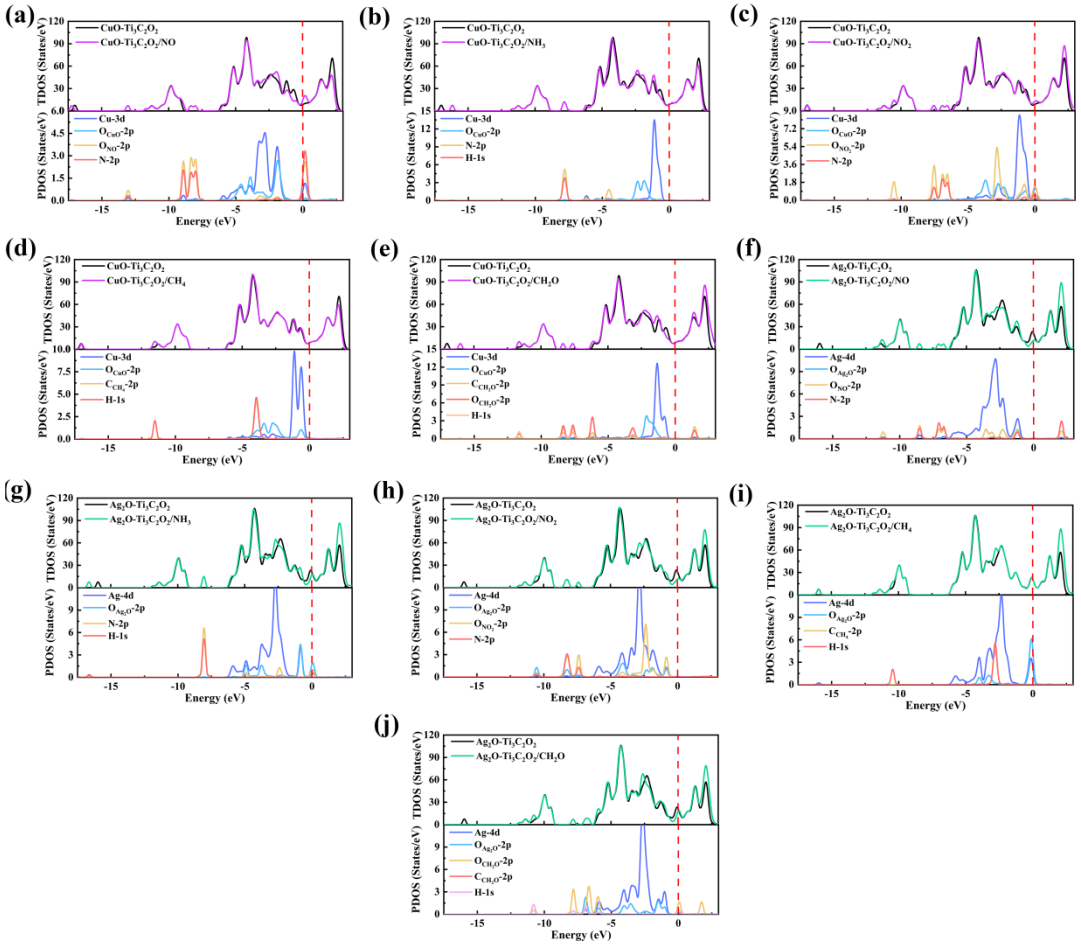


Figure 7. TDOS and PDOS of five gases at (a-e) Ti-O-Cu-C and (f-j) O-Ag-O-Ag-O.

To further analyze the effect of five gas molecules adsorbed on Ti-O-Cu-C and O-Ag-O-Ag-O, the calculation of ELF is shown in Figure 8. ELF helps to gain a deep understanding of the disparity in adsorption strength of gas molecules, which more instinctively reflects the bonding characteristics [34]. In the ELF results, the red area indicates charge accumulation and the blue area indicates charge depletion, where 1.00 indicates that the electrons are completely localized and 0.5 indicates that the electrons are completely delocalized. Figure 8b and Figure 8e show the bonding interaction between $NH_3$ and $CH_2O$ gas molecules and Cu atoms. However, there is no bonding interaction between Cu atoms and O atoms. When $NH_3$ gas exists, the bond between Cu atoms and O atoms is broken, which is not conducive to reuse. Figure 8d, Figure 8g and Figure 8i show that there is no bonding between the gas and the substrate, consistent with small $E_{ads}$. This means that the adsorption process is reversible. Figure 8a, Figure 8c, Figure 8f, and Figure 8h show that the ELF value of N atoms in NO gas molecules and O atoms in $NO_2$ gas molecules is about 0.8, which is in an electron localization state. It is speculated that there may be existence strong interaction between atoms, consistent with DOS. Supporting the above analysis: CuO and $Ag_2O$ modified $Ti_3C_2O_2$ are suitable for adsorbing NO and $NO_2$ respectively.

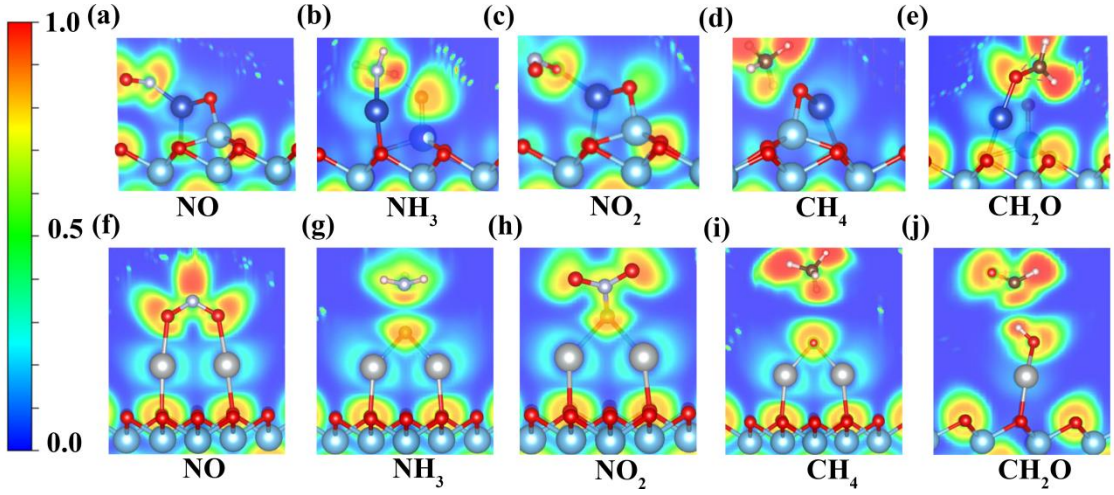


Figure 8. ELF of five gases at (a-e) Ti-O-Cu-C and (f-j) O-Ag-O-Ag-O.

It can be seen that adequate charge is transferred during the reaction of substrates with gas, in Figure 9. In Figure 9a, $NO_2$ loses a larger charge of 0.327 e from Ti-O-Cu-C. The substrates surface has the weakest interaction with $CH_4$ of all the gas adsorption reactions (-0.015 e and -0.005 e). Of particular note, the almost unchanged TDOS in

Figure 7d and Figure 7i indicate low detection sensitivity for $CH_4$ on substrates, which corresponds to less charge transfer in Figure 9, which is consistent with the previous analysis of $CH_4$ physical adsorption is consistent.

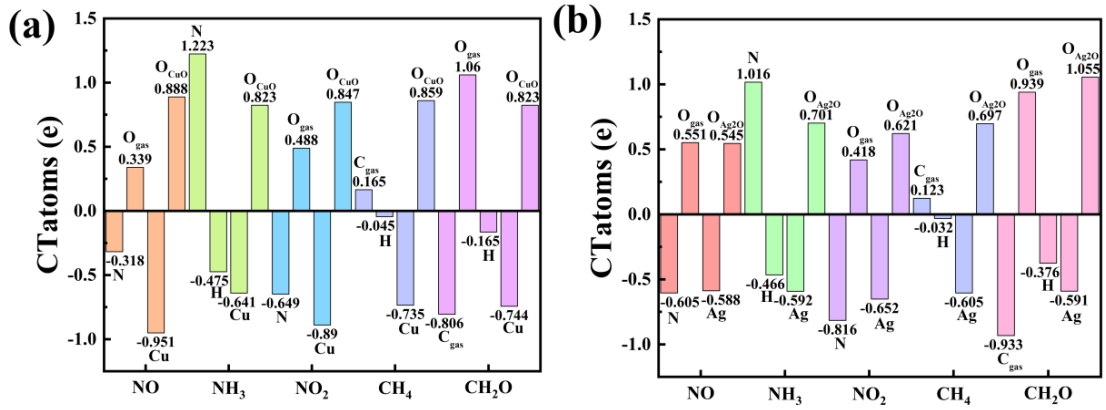


Figure 9. Average charge transfer of five gases at (a) Ti-O-Cu-C and (b) O-Ag-O-Ag-O.

*3.3 Adsorption properties in different systems*

As a gas sensor, various gas models should be compared for their desorption performance on the gas sensor applications. The desorption time τ represents the time required to remove gas molecules adsorbed on the surface of the material. It is also an important parameter for sensing performance. Its characteristic is the desorb time, which is generally calculated by Equation 4:

$$\tau = A^{-1}\exp(E_a/k_BT) \quad (4)$$

Among them, A ($S^{-1}$) is the apparent frequency factor and the value of A is evaluated as $10^{12}$ $s^{-1}$ [35,36]; T is the temperature, which can be set according to the required temperature; $E_a$ (eV) represents the absolute value of the adsorption energy. As is shown in the equation the greater the adsorption energy of gas molecules, the more difficult it is to desorb. The desorption time obtained at the temperature of 298 K, 348 K, and 398 K are plotted in Figure 10.

The adsorption energies of $CH_4$ and $CH_2O$ on Ti-O-Cu-C and $NH_3$ and $CH_4$ on O-Ag-O-Ag-O are relatively small, reflecting the less desorption time. The minimum desorption time of $CH_4$ on Ti-O-Cu-C and O-Ag-O-Ag-O is 24.9 ns and 14.4 ns respectively, and the temperature is 298 K. The desorption time indicates that the desorption process of gas molecules on the substrate can easily occur, and the

adsorption interference to other gases is small. The desorption time of Ti-O-Cu-C for NO gas shortens as the temperature increases. When the temperature is 398 K, the desorption time is $1.69 \times 10^6$ s, which can be used to remove NO. At a temperature of 398 K, the desorption time of $NO_2$ on O-Ag-O-Ag-O is $2.67 \times 10^{23}$ s, and it takes a long time for $NO_2$ to desorpt from the material surface. The adsorption intensity of the above two gases is still very high at 398 K, and CuO and $Ag_2O$ modified $Ti_3C_2O_2$ are very suitable as adsorbents.

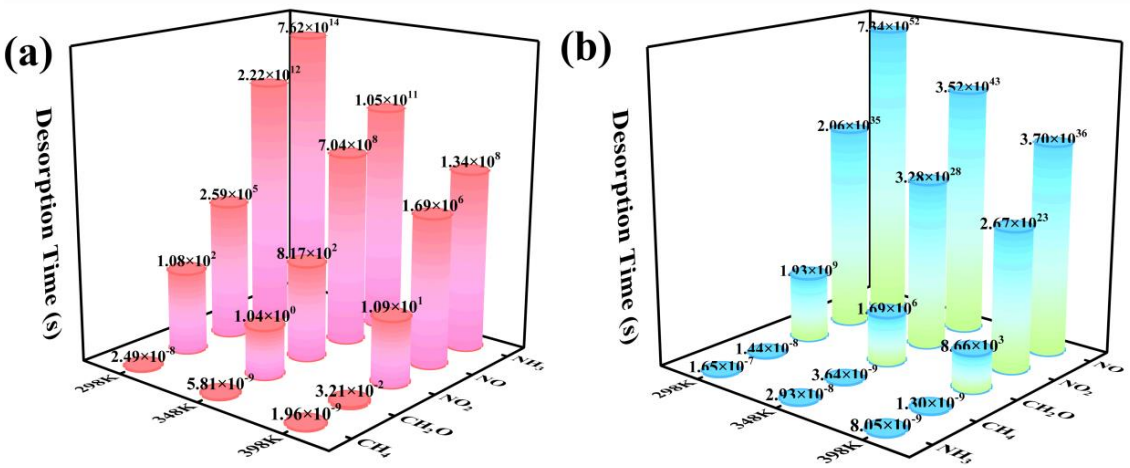


Figure 10. The calculated desorption time of five gases at (a) Ti-O-Cu-C and (b) O-Ag-O-Ag-O.

## 4. Conclusion

In summary, the adsorption energies and electronic properties of NO, $NH_3$, $NO_2$, $CH_4$, and $CH_2O$ gas molecules on CuO/$Ag_2O$modified $Ti_3C_2O_2$ were calculated and compared. The results show that CuO/$Ag_2O$ modification of $Ti_3C_2O_2$ can significantly improve the adsorption of gas on the surface of $Ti_3C_2O_2$. The high adsorption energy (-1.44 eV) of the CuO-modified $Ti_3C_2O_2$ system makes the adsorption chance of NO higher, and the high adsorption energy (-2.80 eV) of the $Ag_2O$-modified $Ti_3C_2O_2$ system makes the adsorption chance of $NO_2$ higher. The adsorption time shows that CuO and $Ag_2O$ modified $Ti_3C_2O_2$ has broad application possibilities in adsorbing NO and $NO_2$, and provides a theoretical analysis of its gas-sensing mechanism. Therefore, CuO, $Ag_2O$ modified $Ti_3C_2O_2$ can be considered suitable oxynitride gas-sensing materials.

**Acknowledgements**

This work was supported by National Natural Science Foundation of China (No.52102164), Heilongjiang Province Natural Science Foundation of China (No. ZD2023E006), Harbin manufacturing science and technology innovation talent project (No.2022CXRCCG00)；Project to Enlist Young Scientific and Technological Talents in Heilongjiang Province (2022QNTJ004).

## Reference


[1] Z. Du, D. Denkenberger, J. M. Pearce, Sol. Energy **2015**, 122, 562.

[2] X. Liu, L. Yin, X. Deng, D. Gong, S. Du, S. Wang, Z. Zhang, J. Hazard. Mater **2020**, 395, 122679.

[3] K.R. Ellsworth, M.A. Ellsworth, A.L. Weaver, K.C. Mara, R.H. Clark, W.A. Carey, JAMA Pediatr **2018**, 172, e180761.

[4] O. Ghaffarpasand, D.C. Beddows, K. Ropkins, F.D. Pope, Sci. Total Environ **2020,** 734, 139416.

[5] J. Gasparotto, K.D.B. Martinello, Energy Geoscience **2021**, 2, 113.

[6] A.V. Agrawal, N. Kumar, M. Kumar, Nanomicro Lett **2021**, 13, 1.

[7] A. Singh, S. Sikarwar, A. Verma, B.C. Yadav, Sens. Actuator A Phys **2021**, 332, 113127.

[8] P. Srinivasan, S. Samanta, A. Krishnakumar, J.B.B. Rayappan, K. Kailasam, J. Mater. Chem. A **2021**, 9, 10612.

[9] X. Liu, H. Zhang, C. Liu, Z. Wang, T. Shen, Phys. Status Solidi **2022**, 219, 2200243.

[10] L. Kong, X. Liang, X. Deng, C. Guo, C. M. L, Adv. Theory Simul. **2021,** 7, 2100074.

[11] F. Zeng, H. Qiu, X. Feng, X. Chao, L. Dai, Q. Yao, J. Tang, Nanomaterials **2022**, 12, 2311.

[12] K. Weng, J. Peng, Z. Shi, A. Arramel, Neng, L, ACS Omega **2023**, 8, 4261.

[13] Y. Miao, G. Pan, C. Sun, P. He, G. Cao, C. Luo, L. Zhang, H. Li, Sens. Rev **2018**, 38, 311.

[14] A.E.A.A. Said, M. Abd El Aal, Res. Chem. Intermed **2017**, 43, 3205.

[15] M. Mansha, A. Qurashi, N. Ullah, F.O. Bakare, I. Khan, Z.H. Yamani, Ceram **2016**, 42.9, 11490.

[16] Mohammadi-Manesh E, Vaezzadeh M, Saeidi M. Surf. Sci **2015**, 636, 36.

[17] He X, Gui Y, Xie J, Liu X, Wang Q, Tang C. Appl. Surf. Sci **2020**, 500, 144030.1.

[18] Ayesh A I, Ahmed R E, Al-Rashid M A, Rafah A A, Belal S, Tahir A, Yousef H, Leena A A. Sens. Actuator A Phys **2018**, 283, 107-112.

[19] Ghasemi A R, Doroodmand M M, Sheikhi M H, Nasresfahani S, J. nanoeng. nanomanuf **2013**, 3, 202-210.

[20] G. Kresse, J. Furthmüller, Comput. Mater. Sci **1996**, 6.1, 15.

[21] G. Kresse, D. Joubert, Phys. Rev. B **1999**, 59.3, 1758.

[22] M. Ernzerhof, G E. Scuseria, J. Chem. Phys **1999**, 110.11, 5029.

[23] Y S. Lin, G D. Li, S P. Mao, J D. Chai, J. Chem. Theory Comput **2013**, 9.1, 263.

[24] B. Xiao, Y. Li, X. Yu, J. Cheng, Sens. Actuators B Chem **2016**, 235, 103.

[25] V. Wang, N Xu, J C. Liu, G. Tang, W. Geng, Comput. Phys. Commun **2021**, 267, 108033.

[26] M. Yu, D R. Trinkle, J. Chem. Phys **2011**, 134.6, 064111.

[27] W. Tang, E. Sanville, G. Henkelman, J. Phys. Condens. Matter **2009**, 21.8, 084204.

[28] E. Sanville, S D. Kenny, R. Smith, G. J Comput Chem **2007**, 28.5, 899.

[29] G. Henkelman, A. Arnaldsson, H. Jónsson, Comput. Mater. Sci **2006**, 36.3, 354.

[30] C. Wang, H. Yang, F. Chen, L. Yue, Z. Wang, B. Xing, Environ. Sci. Technol **2021**, 55.18, 12317.

[31] T. Hu, Z. Li, M. Hu, J. Wang, Q. Hu, Q. Li, X. Wang, J. Phys. Chem. C **2017**, 121.35, 19254.

[32] X. Zhang, Y. Chen, Z. Yang, J. Phys. D Appl. Phys **2018**, 51, 345304.

[33] X. Deng, X. Liang, S.P. Ng, C.M. Lawrence, Appl. Surf. Sci **2019**, 484, 1244.

[34] A. Feng, Y. Yu, F. Jiang, Y. Wang, L. Mi, Y. Yu, L. Ceram. Int **2017**, 43, 6322.

[35] Y.H. Zhang, Y.B. Chen, K.G. Zhou, C.H. Liu, J. Zeng, H.L. Zhang, Y. Peng, Nanotechnology **2009**, 20, 185504.

[36] K. Patel, B. Roondhe, S.D. Dabhi, P.K. Jha, J. Hazard Mater **2018**, 351, 337.